Journal of Materials Chemistry A

ARTICLE

Vertically aligned carbon fibers as supporting scaffolds for phase change composites with anisotropic thermal-conductivity and good shape-stability

Received 00th January 20xx,
Accepted 00th January 20xx

DOI: 10.1039/x0xx00000x

www.rsc.org/

Nan Sheng,[a] Ruijie Zhu,[a] Kaixin Dong,[a] Takahiro Nomura,[a] Chunyu Zhu,[a] * Yoshitaka Aoki,[a] Hiroki Habazaki,[a] Tomohiro Akiyama [a]

The wide application of organic phase change materials for thermal energy storage and management are limited by their low thermal conductivity and poor shape-stability. In this work, anisotropically thermal conductive and shape-stabilized phase change composites (PCCs) were successfully prepared with vertically aligned carbon fibers as supporting scaffolds. The aligned and hollow carbon fiber scaffolds with different densities were facilely fabricated by the direct carbonization of rolled cotton sheets with aligned and hollow cellulose fibers. PCCs were obtained by vacuum impregnation of paraffin wax. Because of the interconnected hollow carbon fiber frameworks with vertically aligned fibers and high porosity, the PCCs present enhanced anisotropic thermal conductivity and good shape-stability against leakage. The thermal conductivity from the axial direction along the fibers is higher than that from the lateral direction, since that the aligned fiber scaffolds are acting as the thermal conducting pathway. The thermal conductivity of the PCC with a carbon ratio of 8.8wt% is 0.77 W k^{-1} m^{-1} (> 3 times of pure paraffin) from axial direction, while the value from the lateral direction is 0.58 W k^{-1} m^{-1}. This work provides a novel strategy for designing anisotropically thermal conductive and shape-stable PCCs with potential applications in advanced thermal management and storage.

Keywords: phase change material, thermal energy storage, carbon fiber, anisotropic, thermal conductivity, thermal management

1. Introduction

Thermal energy storage (TES) systems have the potential to increase the energy utilization efficiency and to alleviate the mismatch between the peaks of energy supply and demand. TES has shown diverse applications in industrial plants, power systems, solar thermal energy storage, and thermal management systems and buildings. As compared with conventional sensible heat storage, the use of latent heat phase change materials (PCMs) for TES is especially promising, which has the advantages of high energy density, reduced temperature fluctuation and repeated use with long-term durability. As for latent heat storage, thermal energy is stored or released during the melting or solidifying phase transition process of a PCM. [1-3] So far, organic PCMs, such as paraffin wax (PW), fatty acids and polyethylene glycol, have been extensively investigated for thermal storage and management. These PCMs have shown advantages such as good storage capability, high chemical reliability, low corrosiveness and easy availability. However, the biggest problems of leakage in the process of solid to liquid phase transition and the low thermal conductivity of pure PCMs have limited their direct use for thermal storage and management. [4-6]

To solve the above problems of pure organic PCMs, phase change composites (PCCs) have been fabricated by incorporating various functional supporting and additive materials. To overcome the leakage problem, PCCs have been prepared by impregnating PCMs into porous matrices, such as exfoliated graphite and natural minerals, and by the microencapsulation with polymer or inorganic materials. [7-13] To increase the thermal conductivity of PCCs, thermally conductive additives such as metallic particles, boron nitride,

[a] *Faculty of Engineering, Hokkaido University, Sapporo, Hokkaido 060-8628, Japan. Corresponding author Chunyu ZHU, E-mail: (chunyu6zhu@eng.hokudai.ac.jp)*
† Footnotes relating to the title and/or authors should appear here.
Electronic Supplementary Information (ESI) available: [details of any supplementary information available should be included here]. See DOI: 10.1039/x0xx00000x

alumina, carbon nanotubes, carbon fibers and so on, have been introduced to the PCMs. [9, 14-17] Porous materials such as perlite, diatomite, silica, expanded graphite, metallic foams and various porous carbons, which have the features of both high thermal conductivity and shape-stability, are promising supporting frameworks for PCCs. These porous supporting scaffolds can simultaneously enhance the thermal conductivity and prevent the leakage of liquid PCMs. [4, 6, 14, 15, 18-21] The porous frameworks can work as a shape stabilizer and reservoir of liquid PCMs due to the capillary and surface tension forces of the porous structure. Carbon-based supporting frameworks are especially promising because of their large specific surface area, high porosity, high thermal conductivity and light weight. So far, graphene-based aerogels or foams, graphite foams, and carbon fiber or carbon nanotube aerogels have been used. [22-26] As for a porous framework consisting of fibrous elements, the aligned arrangement of fibers can greatly enhance the thermal conductivity in the axial direction along the fibers, leading to anisotropic thermal conductivity of PCCs.

In this study, we report a facile preparation of anisotropically thermal conductive and shape-stabilized paraffin-based PCCs, which are supported by vertically aligned carbon fiber scaffolds. These supporting scaffolds are derived from low-cost biomass raw material. The aligned carbon fiber scaffolds are facilely fabricated by the direct carbonization of rolled cotton sheets with aligned cellulose fibers. The anisotropically thermal conductive property and the thermal storage performance of the PCCs are carefully investigated.

2. Experiment

2.1 Preparation of aligned carbon fiber frameworks and PCCs.

Commercially available absorbent cotton sheet with a weight density of around 11-12 mg cm^{-2} was used as the raw material for producing carbon fiber frameworks. The cotton sheet was obtained after the combing procedure, which had well aligned fibers. The combed cotton sheet was cut to a width of 5 cm in the fiber direction and length of 18 or 36 cm. The cut cotton sheets were rolled to form cotton rods with the fibers aligning along the axis direction as shown in Figure 1. The rolled cotton rods were fixed by bandaging with gauze cloth. Three cotton rods with different densities were obtained. Sample 1 (S1) was obtained from a cotton sheet with a size of [length 18 cm × width 5 cm], which was rolled in its dry state to form a rod with a diameter of 2 cm; sample 2 (S2) was obtained from a cotton sheet with a size of [length 36 cm × width 5 cm] in the same way; sample 3 (S3) was obtained from a cotton sheet with a size of [length 36 cm × width 5 cm], which was rolled in its wet state to form a compact rod with a diameter of 1.4 cm. The above three cotton rods were firstly pre-pyrolyzed at 500 ºC for 1 h under Ar flow, and further carbonized at 2400 ºC. In this manner, three black carbon rods were obtained, as shown in Figure 1.

The above carbon rods were putted into the liquid PW in a container under vacuum heating at 100 ºC for 2 h. Subsequently, the container consisting of excess liquid PW and cotton rods were cooled to room temperature. Finally, the PW@carbon composites (named as S1@PW, S2@PW, S3@PW) were obtained by peeling off the outside PW. These composites were also cut and shaped to disks with diameters of 10 mm for thermal conductivity measurement.

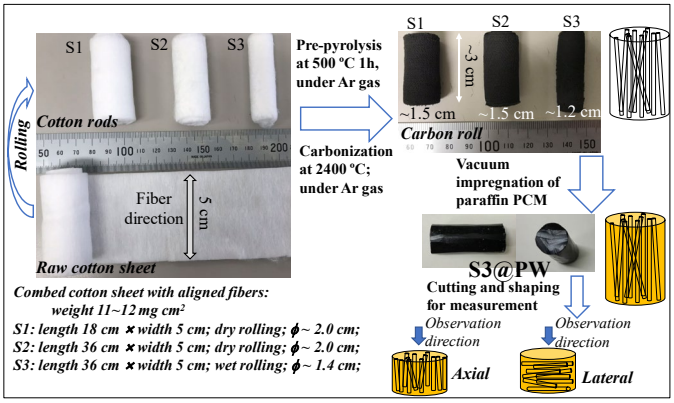

Figure 1. Schematic diagram for producing carbon fiber scaffolds and PCM/carbon composites.

2.2 Material characterization and thermal property measurement

The morphology and microstructure of the samples were observed by scanning electron microscope (SEM, JSM-7500F, JEOL) and transmission electron microscope (TEM, JEM-2010 F). The phase composition of the samples was measured by an X-ray diffractometer (Rigaku MiniFlex600) equipped with Cu Ka radiation. Raman spectra of the carbon sample were acquired using a RENISHAW Raman spectrometer using an excitation wavelength of 532 nm.

The PW loading ratios in the PCCs were determined by comparing the weights before and after impregnation and by thermal gravimetric (TG, Mettler Toledo) analysis under air flow. The density of the PCC samples was obtained by a pycnometer (Quantachrome Instruments, Ultrapycnometer 1000). The thermal conductivity of the samples was obtained based on the Laser Flash method, as described in previous study. [27] Each sample was measured for 5 times to obtain an average value. The thermal conductivity from both the axial and lateral direction were measured. The definition of the axial and lateral direction is shown in Figure 1.

The phase change temperature, enthalpy and cycling stability of the PCCs and PW were measured by differential scanning calorimetry (DSC, METTLER TOLEDO DSC823) with a heating/cooling rate of 10 °C min^{-1}. Leakage test of the PCCs in comparison with PW was carried out by heating the samples above the melting point of PW (80 ºC) for a series of durations.

3. Results and discussion

3.1 Structure and morphology characterization of the carbon framework

Figure 1 shows the schematic diagram for the preparation of cotton-derived carbon frameworks and PCCs. The cotton rods show shrinkage of volume after pyrolysis and carbonization as compared with the original cotton rods, which is due to the release of a lot of gases. The obtained carbon rods are lightweight like a sponge. Furthermore, the carbon rods are also well shaped, which do not spread out or break.

XRD pattern and Raman spectrum of the carbon sample with a carbonization temperature of 2400 ºC are shown in Figure 2. The XRD pattern of the carbon sample displays two distinct peaks locating at around 26 ° and 44 °, which correspond to carbon (002) and (100) planes, respectively. Raman spectrum of the carbon sample shows well-separated and sharp peaks of D-band and G-band, indicating the well graphitization of carbon at 2400 ºC. Here D-band represents the A_{1g} vibration mode of the disordered carbon, while G-band is related to the E_{2g} vibration mode of the ordered graphitic carbon.

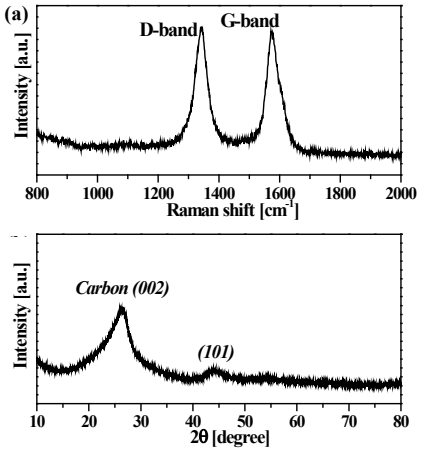

Figure 2. Raman spectrum (a) and XRD pattern (b) for the cotton-derived carbon at 2400 ºC.

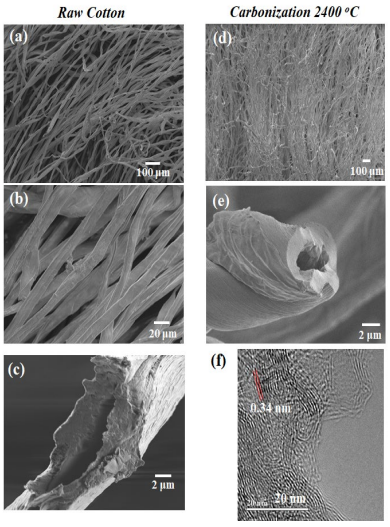

Figure 3. Morphology and structural analysis. SEM images of the original cotton fibers (a, b, c) and carbon obtained at 2400 ºC (d, e). (f) is the high resolution TEM image of the carbon.

Figure 3 shows the morphology and microstructure of the original cotton and carbon obtained at 2400 ºC. From the SEM images (Figure 3-(a,b)), the original cotton sheets are consisted of

cotton cellulose fibers with diameters of dozens of micrometers, which are well aligned in the same direction. The length of a single cotton fiber is as long as several centimeters. In addition, the original cotton fibers are hollow (Figure 3-(c)), which is consistent with previous study. [28] After carbonization at 2400 ºC (Figure 3-(d,e)), the carbon fibers retain their hollow structure. Importantly, the carbon fibers are also well aligned just as the original cotton fibers, indicating the successful preparation of aligned carbon fiber scaffolds. It is also noted that the carbon fibers are not 100% vertically aligned, which are also somewhat curved and crosslinked. This is very important for their form-stability that is proper to be used as the supporting scaffold for PCMs. The high resolution TEM image of the carbon fiber is shown in Figure 3-(f). Many fringes corresponding to graphite (002) planes are observed, representing the well carbonization the cellulose fiber.

3.2 Properties of the PCCs

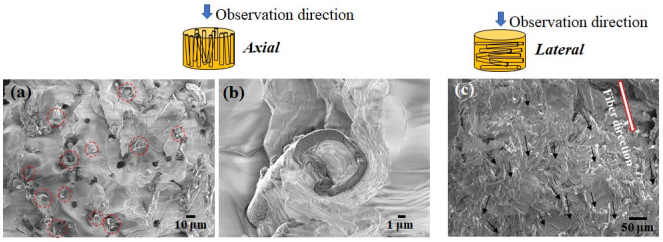

Figure 4. Typical SEM images of the paraffin/carbon composites observed from the axial block (a, b) and lateral block (c).

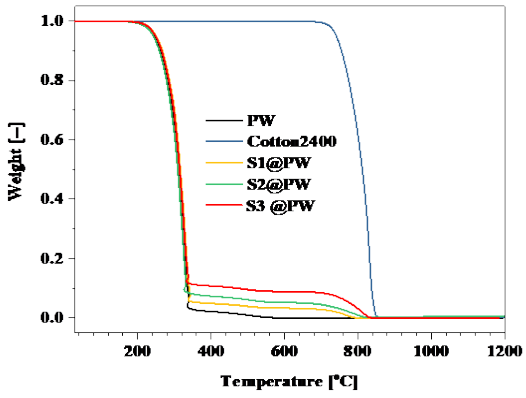

Figure 5. TG curves for the samples obtained under air flow.

As described previously, the carbon rods are lightweight like a sponge, which contain numerous pores including the hollow holes of the fibers and the spaces between the crosslinked fibers. These characteristics could reinforce the impregnation of large amount of PW to form PCCs with high energy storage density. The PCCs were prepared by vacuum impregnation of PW into the aligned carbon fiber scaffolds at 100 ºC. The densities for PW and PCCs are measured to be 0.882, 0.906, 0.916 and 0.933 g cm^{-3} for PW, S1@PW, S2@PW, and S3@PW, respectively. The density of the PCCs is increased as the additive amount of carbon supporting scaffold since that carbon has a higher bulk density than PW. Figure 4 shows the typical SEM images of the PCCs supported by aligned carbon fiber scaffolds. Figures 4-(a,b) present the images obtained from the axial direction of the PCC rod. The cross-section of the hollow carbon fibers can be observed. The fiber holes and the spaces between the fibers are filled with PW, representing the successful preparation of PCCs. As seen from the lateral direction of the PCC in Figure 4-(c), the aligned carbon fibers along the axial direction of the rod are observed.

TG air combustion analysis was used to confirm the thermal stability of the carbon framework and the precise PW contents in the PCCs. The TG analysis was conducted under air flow at a heating rate of 10 °C min^{-1}. Figure 5 shows the TG curves for the air combustion of PW, cotton-derived carbon at 2400 °C, S1@PW, S2@PW, and S3@PW. PW is combusted in the temperature range of around 190~350 °C, while the carbon fibers have a good stability which is combusted at higher than 700 °C. As for the PCCs, the TG curves present two obvious weight decreases in the range of 190~350 °C and higher than 700 °C, corresponding to the combustion of PW and carbon fibers, respectively. By calculating the weight difference ratios between the two reactions, the PW contents in the PCCs were calculated. The weight ratios of PW in PCCs from TG analysis are 96.8%, 94.8% and 91.2% for S1@PW, S2@PW, and S3@PW, respectively. These ratios are similar to those as calculated from the weight changes of the carbon rods before and after PW loading.

3.3 Thermal conductivity and heat transfer properties of the PCCs

A major drawback of organic PCMs is their low thermal conductivities which can reduce the heat transfer rates and restrain their practical applications. PW has a low thermal conductivity of 0.25 W k^{-1} m^{-1}. Therefore, it is essential to increase the thermal conductivity of paraffin. The carbon-based supporting frameworks are expected to increase the thermal conductivity of as-prepared PCCs. The thermal conductivities of the PCCs as-supported by aligned carbon fiber scaffolds were measured from both the axial and lateral directions. Figure 6 shows the thermal conductivities for the PCCs in comparison with PW. The measured thermal conductivities are 0.33, 0.46 and 0.58 W k^{-1} m^{-1} from the lateral direction and are 0.44, 0.62 and 0.77 W k^{-1} m^{-1} from the axis direction for samples S1@PW, S2@PW and S3@PW, respectively. The thermal conductivity of the PCCs increases as the carbon additive ratios in the PCCs. The value of 0.77 W k^{-1} m^{-1} for sample S3@PW from the axial direction is more than 3 times of that of PW. The aligned carbon fiber scaffolds supported PCCs also present anisotropically enhanced thermal conductivity. The values of the thermal conductivity from the axial direction is about 1.33 times of that from the lateral direction. This is caused by the vertically aligned carbon fibers, which are employed as the thermal conducting pathway in the PCCs. Definitely, the thermal conductance is less disturbed along the fibers in the axial direction than from the lateral direction between the fibers.

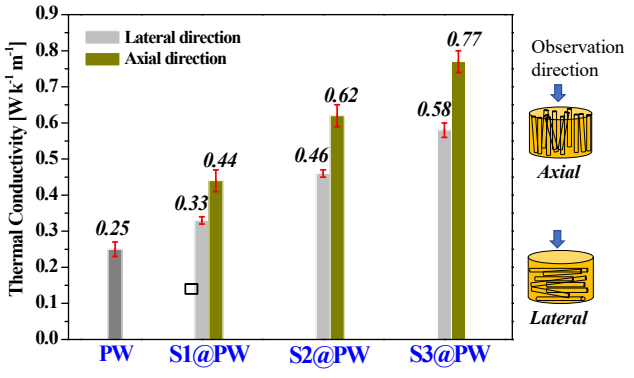

Figure 6. Thermal conductivity of the PCCs in comparison with PW. The thermal conductivity for the PCCs along the axial direction (fiber direction) and lateral direction were compared. Inset shows the average values for each sample.

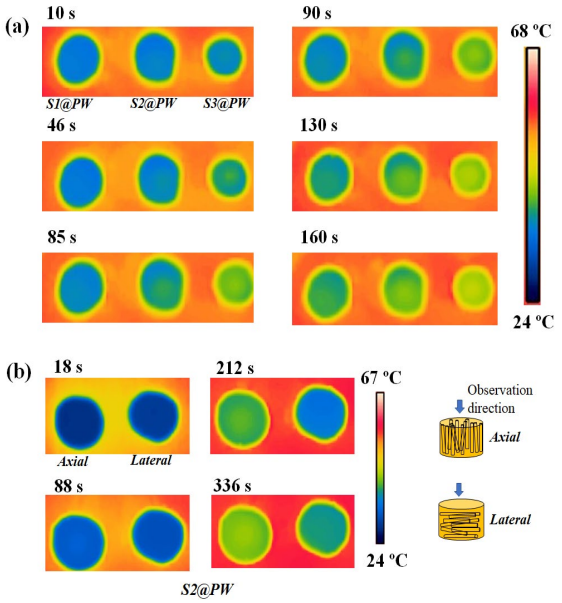

Figure 7. Thermal images of the samples during heating. (a) Three composites from axial direction; (b) composite S2@PW from both axial and lateral directions.

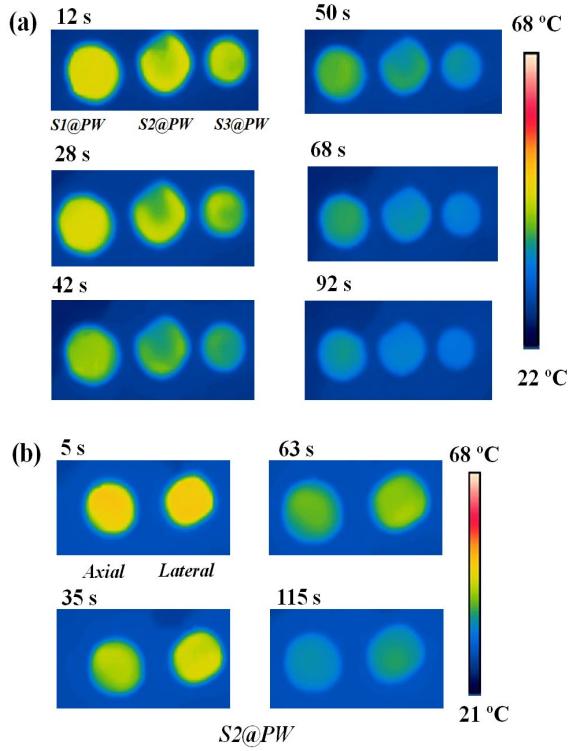

Figure 8. Thermal images of the samples during cooling. (a) Three composites from axial direction; (b) composite S2@PW from both axial and lateral directions.

To directly observe the heat transfer rate and heat dissipation capability during thermal energy storage and management, an infrared camera was used to record the transient temperature response during heating and cooling, corresponding to the thermal storage and release processes, respectively. For the heating process, the composite samples were put on an isothermal ceramic plate as heated on a hot plate at 80 ºC. The infrared thermal images with temperature distribution of the PCCs at different heating durations are shown in Figure 7. For the cooling process, the comparable samples were firstly heated at on a hot plate at 80 ºC for a certain duration. Subsequently, the samples were quickly transferred to an isothermal ceramic plate at room temperature and the temperature responses during the cooling process were recorded as shown in Figure 8. Figure 7-(a) presents the thermal images of the three PCCs with different carbon ratios as observed from the axial direction. It is clearly seen that, with the increase of carbon density in the composites, the PCCs demonstrate faster temperature increase. The samples present temperature increasing rate in a sequence of S3@PW > S2@PW > S1@PW. This result indicates the importance of the carbon framework on enhancing the thermal transport of the PCCs, which is employed as the thermal conducting pathway. Definitely, a higher density of carbon framework is beneficial to a higher heat transfer rate. Figure 7-(b) shows the comparison of thermal images for sample S2@PW, which were taken from both the axial and lateral blocks. Obviously, the axial block presents higher temperature images than the lateral one, indicating the anisotropically enhanced thermal conductivity along the fiber direction. As for the cooling process shown in Figure 8-(a), with the increase of carbon density in the PCCs, the samples present faster temperature decrease due to the assistance of thermal dissipation by the carbon network. The comparison of the cooling temperature response for the axial and lateral blocks for sample S2@PW is shown in Figure 8-(b), in which the axial block shows faster temperature decrease than the lateral one. This further confirms that the aligned carbon fibers are beneficial to the anisotropically enhanced thermal conductivity along the fiber direction.

The high thermal conductivity and high rate of thermal response for the composites as supported by our carbon fiber scaffolds, especially from the axial fiber direction, enable the paraffin-based PCCs to absorb/release thermal energy quickly during phase changes. The working efficiency of these PCCs can be greatly improved when they are used for thermal storage and management. In addition, the successful preparation of the anisotropically enhanced thermal conductive PCCs can provide more possibilities for designing various thermal storage and management systems that need anisotropic thermal conductivity, for example in application for the thermal dissipation of electronic devices.

3.4 Phase change properties of PCCs

The phase change properties including phase change temperatures, specific phase change enthalpies, and phase change cyclability of the PCCs and PW were measured using DSC. Figure 9 shows the typical heating and cooling DSC curves of PW and PCCs. Two phase change peaks during both the melting and solidification processes are observed for all samples, representing the typical solid-solid and solid-liquid phase change of paraffin. Because of the confinement effect of the porous media, the melting curves for the composite samples show shift to higher temperature side while the solidification curves show shift to lower temperature side, as compared to the pure PW.[15, 18] Phase change enthalpy is the most reliable indicator for the assessment of the thermal energy storage capacity of PCCs. The phase change enthalpies are 217.7 J g^{-1} and 215.4 J g^{-1} for PW during the melting and solidification processes, respectively. The values of phase change enthalpies of the composite samples are decreased as the increase of carbon weight ratio in the composites. As for sample S3@PW with the largest carbon amount of 8.8%, the values are 199.4 J g^{-1} and 199.2 J g^{-1} for the melting and solidification processes, respectively. These measured values are similar to the calculated values of theoretical enthalpies by considering the weight of carbon in the PCCs. The phase change temperatures and enthalpies are summarized in Table 1.

The composite samples also show good phase change cycling stability, which were measured by repeating the melting and solidification processes in the DSC apparatus up to 100 cycles. The DSC curves during the 100 cycles are almost overlapped for all samples (Figure 9), and the phase change enthalpies and phase change temperatures are stable for all samples. The phase change temperatures and enthalpies after 100 cycles are also shown in Table

1, which are similar to their initial values before cycling. Figure 10 presents the changes of the phase change enthalpies with an example of sample S2@PW during 100 cycles, and the values are very stable both for melting and solidification processes. The XRD patterns of original PW and the PW@C before/after cycling are shown in Figure 11. The peaks for three samples are identical, indicating the good chemical structure stability of PW after cycling. Therefore, the PCCs are proper for repeating thermal storage/release cycling. The good phase change cycling stability and chemical stability of the samples could reinforce their application for long-term thermal energy storage through repeated use.

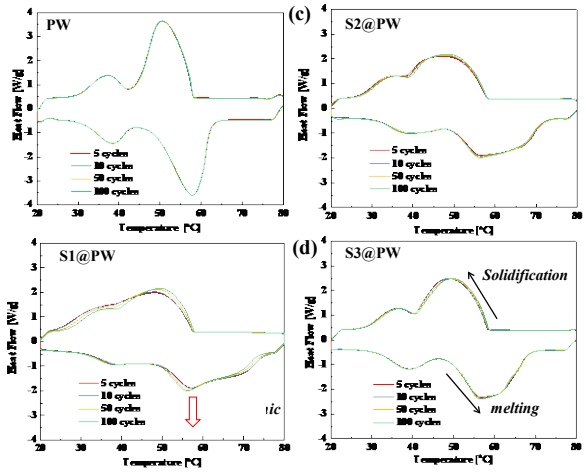

Figure 9. DSC curves of the heating and cooling process of PW and PCCs.

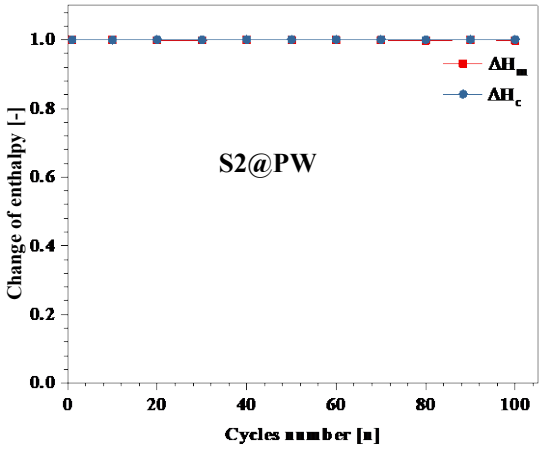

Figure 10. Phase change stability of PCC. The typical latent heat change during 100 cycles for sample S2@PW. The other samples show the same tendency with this sample.

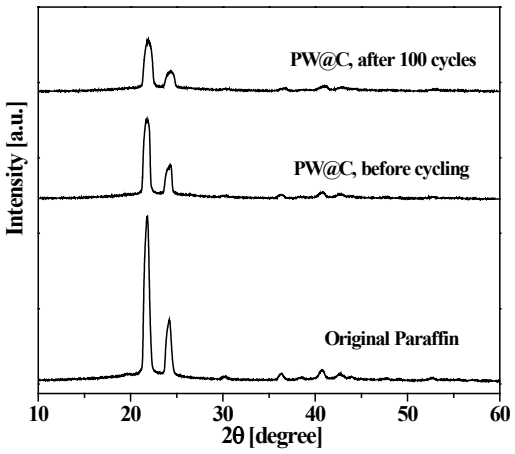

Figure 11. XRD patterns of PW and PW@C before/after cycling.

3.5 Shape-stability (leakage-proof property) of the PCCs

The shape-stability, also known as the leakage-proof property, of PCCs was confirmed by heating the samples in an 80 ºC furnace as compared with PW. The pictures of the samples were taken by a digital camera at different heating durations, as shown in Figure 12. All samples were solid in their initial stage of heating. After several minutes of heating, paraffin began to melt, and after 30 min of heating the PW sample was totally melted that spread over the container. However, the PCCs samples can almost keep their original shape with the liquified paraffin confining in the porous carbon scaffolds. It is noted that there is a small amount of paraffin that leaked from the bottom of the PCCs after heating for 30 min (Figure 12-(a)). This is inescapable due to the outside paraffin on the surface around the porous carbon rods. Here, the PCCs as-shown in Figure 12-(a) were prepared by vacuum impregnation at 100 ºC by putting the porous carbon rods into the liquid paraffin; subsequently, the liquid PW containing the carbon rods were cooled to room temperature; finally, the outside solidified paraffin around the

carbon rods was carefully peeled off. In this way, there are no pores in the PCCs, which is beneficial to the correct measurement of thermal conductivity. In fact, the PCCs without excess surface paraffin were also prepared by a modified procedure: the porous carbon rods were firstly putted into the liquid paraffin under vacuum for 2 h of impregnation; subsequently, the carbon rods containing liquid paraffin were taken out by a mesh spoon to let the surface paraffin leak out; finally, the composites were cooled down to room temperature. In this way, better composites without any leakage on the surface can be obtained, as shown in Figure 12-(b). After heating 30 min, the PW is completely melted and spread out, while the PCC does not show any leakage even when the melted PCC is moved onto a tissue paper.

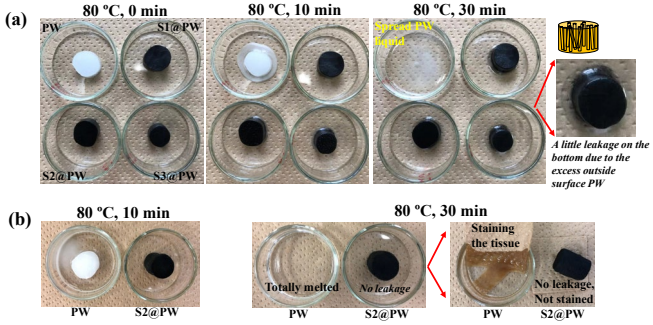

Figure 12. Leakage test of the PCCs and PW. The photographs for the samples heated at 80 ºC to different durations are presented. (a) the PCCs were prepared with some excess surface PW, showing a little leakage on the bottom of PCCs after melting; (b) the PCC was prepared without excess surface PW, showing no leakage.

The above observation reveals that the porous carbon fiber scaffolds can play a role in enhancing the shape-stability of PCCs during phase changes. The shape-stability (leakage-proof) of the PCCs is arose by the adsorption effects, including the capillary force and intermolecular forces, of the hollow carbon fibers and porous scaffolds on paraffin.

Finally, the porous carbon scaffolds are very easily prepared by the direct carbonization of biomass cotton, which has the advantage of low-cost and easy availability. In addition, the cotton-derived framework is also facilely shaped to diverse structures for their wide use. Therefore, we believe that the newly developed porous carbon supporting materials can be widely applied to prepare phase change composites for thermal energy storage and management.

4. Conclusions

In summary, we reported a novel strategy to prepare anisotropically thermal conductive and shape-stable paraffin-based phase change composites, which were supported by porous carbon scaffolds consisting of aligned and hollow carbon fibers. The carbon scaffolds were facilely fabricated by the direct carbonization of rolled cotton sheets, which had aligned and hollow cellulose fibers. Paraffin was impregnated into the porous carbon scaffolds under vacuum heating. Because of the vertically aligned carbon fibers which were serviced as the thermal conducting pathway, the composites presented enhanced anisotropic thermal conductivity. For the composite with a carbon ratio of 8.8wt%, the thermal conductivity is 0.77 W k^{-1} m^{-1} (> 3 times of pure paraffin) from the axial direction, while the value from the lateral direction is 0.58 W k^{-1} m^{-1}. The composites also illustrated good shape-stability against leakage when they were heated to temperatures above the melting point of paraffin, due to the capillary adsorption effects of the hollow carbon fibers and porous scaffolds on liquid paraffin. Additionally, the composites also presented high thermal storage capacity (e.g., 199 J g^{-1} for the composite with a carbon amount of 8.8wt%) and good cyclability. The facile fabrication of anisotropically conductive supporting frameworks from low-cost biomass material can reinforce the applications of phase change composites for advanced thermal management and storage, e.g., the solar thermal energy utilization.

Acknowledgements

The authors thank the “Nanotechnology platform” Program of the Ministry of Education, Culture, Sports, Science and Technology (MEXT) for the use of analysis equipment.

References:

1. A. Dinker, M. Agarwal and G. D. Agarwal, *Journal of the Energy Institute*, 2017, **90**, 1-11.
2. H. Zhang, J. Baeyens, G. Cáceres, J. Degrève and Y. Lv, *Progress in Energy and Combustion Science*, 2016, **53**, 1-40.
3. B. Xu, P. Li and C. Chan, *Applied Energy*, 2015, **160**, 286-307.
4. S. Tahan Latibari and S. M. Sadrameli, *Solar Energy*, 2018, **170**, 1130-1161.
5. E. M. Shchukina, M. Graham, Z. Zheng and D. G. Shchukin, *Chemical Society Reviews*, 2018, **47**, 4156-4175.
6. X. Huang, X. Chen, A. Li, D. Atinafu, H. Gao, W. Dong and G. Wang, *Chemical Engineering Journal*, 2018, **356**, 641-661.
7. Y. Lin, C. Zhu, G. Alva and G. Fang, *Applied Energy*, 2018, **231**, 494-501.
8. F. Wang, Z. Ling, X. Fang and Z. Zhang, *Solar Energy Materials and Solar Cells*, 2018, **186**, 340-348.
9. Y. Zhou, W. Sun, Z. Ling, X. Fang and Z. Zhang, *Industrial & Engineering Chemistry Research*, 2017, **56**, 14799-14806.
10. C. Liu, Z. Rao, J. Zhao, Y. Huo and Y. Li, *Nano Energy*, 2015, **13**, 814-826.
11. K. Yuan, J. Liu, X. Fang and Z. Zhang, *Journal of Materials Chemistry A*, 2018, **6**, 4535-4543.
12. P. Lv, C. Liu and Z. Rao, *Applied Energy*, 2016, **182**, 475-487.
13. T. Wang, S. Wang, R. Luo, C. Zhu, T. Akiyama and Z. Zhang, *Applied Energy*, 2016, **171**, 113-119.
14. D. Zou, X. Ma, X. Liu, P. Zheng and Y. Hu, *International Journal of Heat and Mass Transfer*, 2018, **120**, 33-41.
15. J. Wang, X. Jia, D. G. Atinafu, M. Wang, G. Wang and Y. Lu, *Journal of Materials Chemistry A*, 2017, **5**, 24321-24328
16. T. Sreethawong, K. W. Shah, S.-Y. Zhang, E. Ye, S. H. Lim, U. Maheswaran, W. Y. Mao and M.-Y. Han, *Journal of Materials Chemistry A*, 2014, **2**, 3417-3423.
17. J. Yang, L.-S. Tang, R.-Y. Bao, L. Bai, Z.-Y. Liu, W. Yang, B.-H. Xie and M.-B. Yang, *Chemical Engineering Journal*, 2017, **315**, 481-490.
18. A. Karaipekli, A. Biçer, A. Sarı and V. V. Tyagi, *Energy Conversion and Management*, 2017, **134**, 373-381.
19. R. Luo, S. Wang, T. Wang, C. Zhu, T. Nomura and T. Akiyama, *Energy and Buildings*, 2015, **108**, 373-380.
20. P. Zhang, Z. N. Meng, H. Zhu, Y. L. Wang and S. P. Peng, *Applied Energy*, 2017, **185**, 1971-1983.
21. D. G. Atinafu, W. Dong, C. Wang and G. Wang, *Journal of Materials Chemistry A*, 2018, **6**, 8969-8977.
22. Y. Li, J. Li, W. Feng, X. Wang and H. Nian, *ACS Sustainable Chemistry & Engineering*, 2017, **5**, 7594-7603.
23. H. Ji, D. P. Sellan, M. T. Pettes, X. Kong, J. Ji, L. Shi and R. S. Ruoff, *Energy & Environmental Science*, 2014, **7**, 1185-1192.
24. J. Yang, G.-Q. Qi, R.-Y. Bao, K. Yi, M. Li, L. Peng, Z. Cai, M.-B. Yang, D. Wei and W. Yang, *Energy Storage Materials*, 2018, **13**, 88-95.
25. Q.-Q. Kong, Z. Liu, J.-G. Gao, C.-M. Chen, Q. Zhang, G. Zhou, Z.-C. Tao, X.-H. Zhang, M.-Z. Wang, F. Li and R. Cai, *Advanced Functional Materials*, 2014, **24**, 4222-4228.
26. L. Chen, R. Zou, W. Xia, Z. Liu, Y. Shang, J. Zhu, Y. Wang, J. Lin, D. Xia and A. Cao, *ACS Nano*, 2012, **6**, 10884-10892.
27. T. Nomura, K. Tabuchi, C. Zhu, N. Sheng, S. Wang and T. Akiyama, *Applied Energy*, 2015, **154**, 678-685.
28. B. Wang, R. Karthikeyan, X.-Y. Lu, J. Xuan and M. K. H. Leung, *Industrial & Engineering Chemistry Research*, 2013, **52**, 18251-18261.

Table 1. Data for the thermal properties from DSC of the PCCs and PW.

Samples	Cycle No.	*Melting process*				*Solidification process*			
		T_{mo} (°C)	T_{me} (°C)	T_{mp} (°C)	ΔH_m (J g^{-1})	T_{so} (°C)	T_{se} (°C)	T_{sp} (°C)	ΔH_s (J g^{-1})
PW	**5**	25.5	66.0	57.8	217.7	25.0	58.4	50.5	215.4
	100	25.5	66.0	57.8	217.7	25.0	58.4	50.5	215.3
S1 @ PW	**5**	22.5	77.2	57.3	204.1	22.5	57.5	48.2	201.1
	100	22.5	76.5	55.8	203.6	23.5	58.1	49.6	201.0
S2 @ PW	**5**	24.5	75.7	57.5	201.9	23.0	58.2	47.5	201.3
	100	24.5	75.1	57.5	201.6	23.1	58.2	47.8	201.3
S3 @ PW	**5**	25.0	71.5	57.0	199.4	25.0	58.4	48.8	199.2
	100	25.0	71.5	56.6	199.4	25.0	58.7	49.5	198.8

T_{mo}, T_{me}, T_{mp}, ΔH_m are the onset point, end point, peak temperature and phase change enthalpy during the melting process, while T_{so}, T_{se}, T_{sp}, ΔH_s are the onset point, end point, peak temperature and phase change enthalpy during the solidification process, respectively.